

A High-resolution DOA Estimation Method with a Family of Nonconvex Penalties

Xiaohuan Wu, *Student Member, IEEE*, Wei-Ping Zhu, *Senior Member, IEEE*, and Jun Yan

Abstract—The low-rank matrix reconstruction (LRMR) approach is widely used in direction-of-arrival (DOA) estimation. As the rank norm penalty in an LRMR is NP-hard to compute, the nuclear norm (or the trace norm for a positive semidefinite (PSD) matrix) has been often employed as a convex relaxation of the rank norm. However, solving a nuclear norm convex problem may lead to a suboptimal solution of the original rank norm problem. In this paper, we propose to apply a family of nonconvex penalties on the singular values of the covariance matrix as the sparsity metrics to approximate the rank norm. In particular, we formulate a nonconvex minimization problem and solve it by using a locally convergent iterative reweighted strategy in order to enhance the sparsity and resolution. The problem in each iteration is convex and hence can be solved by using the optimization toolbox. Convergence analysis shows that the new method is able to obtain a suboptimal solution. The connection between the proposed method and the sparse signal reconstruction (SSR) is explored showing that our method can be regarded as a sparsity-based method with the number of sampling grids approaching infinity. Two feasible implementation algorithms that are based on solving a duality problem and deducing a closed-form solution of the simplified problem are also provided for the convex problem at each iteration to expedite the convergence. Extensive simulation studies are conducted to show the superiority of the proposed methods.

Index Terms—Direction-of-arrival (DOA) estimation, gridless method, nonconvex penalties, Toeplitz covariance matrix, low-rank matrix reconstruction.

I. INTRODUCTION

As a fundamental problem in array signal processing, direction-of-arrival (DOA) estimation has been widely employed in many applications, i.e., radar, sonar, speech processing and wireless communications [1]–[3]. The study of DOA estimation problem has been a long history and many methods have been proposed in the past two decades, including some well known conventional methods such as Capon method and the subspace-based methods, e.g., MUSIC (see [4] for a detailed review). MUSIC is equivalent to a large sample realization of the maximum likelihood (ML) method when the signals are uncorrelated, and has a super-resolution compared

to Capon method under certain conditions [5]. However, MUSIC requires the number of sources as *a priori* and a one-dimensional (1-D) searching procedure which is computationally expensive. Moreover, MUSIC faces difficulties in the case of sparse linear array (SLA), especially when the number of sources is greater than that of sensors. Although the root-MUSIC has been proposed for efficiency consideration, it only can be used for the uniform linear array (ULA).

Compressive sensing [6] is a technique of reconstructing a high dimensional signal from fewer samples and has been introduced into the DOA estimation area, resulting in a number of sparsity-based methods for DOA estimation [7]–[11]. The sparsity-based methods exhibit several advantages over subspace-based and the ML methods such as robustness to noise, no requirement for source number, and improved resolution. However, the sparsity-based methods require the DOAs of interest to be sparse in the whole angle space. To this end, the angle space has to be discretized into a finite set of angle grids and the DOAs of interest are assumed to exactly lie on the grids. However, in reality, the DOAs could lie in the continuous infinite set of angles, and hence the assumption holds only when the size of the set tends to infinity, which results in an unacceptable computational cost. Moreover, the discretization strategy may degenerate the performance of the sparsity-based methods as there is often an unavoidable bias between the true DOAs and the predefined grids, which can be interpreted as the basis mismatch issue. To address this issue, several modified off-grid sparsity-based methods have been proposed [12]–[15]. However, these methods are the mitigation measures only, since the discretization still exists which does not eliminate the effect of basis mismatch but bring complexity issue.

Recently, the atomic norm is introduced as a mathematical theory by V. Chandrasekaran *et al.* [16], and then extended for line spectral estimation by Tang in [17]. Since DOA estimation problem actually equates to the frequency recovery problem in the presence of multiple measurement vectors (MMVs) which share the same frequency components, the atomic norm minimization (ANM) technique can be directly applied to the DOA estimation, as explored by Yang in [18]. The ANM can be referred to as a gridless method since it views the DOA estimation as a sparse reconstruction problem with a continuous infinite dictionary and recovers the DOAs by solving a semidefinite programming (SDP) problem. It is shown that the DOAs can be exactly recovered with a high probability provided that they are appropriately separated. Note that since the discretization is not required, ANM is able to eliminate the effect of basis mismatch. However, the DOA

This work was supported by the National Natural Science Foundation of China under grant No. 61372122 and No. 61471205; the Innovation Program for Postgraduate in Jiangsu Province under grant No. KYLX 0813.

X. Wu and J. Yan are with the Key Lab of Broadband Wireless Communication and Sensor Network Technology, Nanjing University of Posts and Telecommunications, Nanjing, 210003, China (e-mail: 2013010101@njupt.edu.cn).

W.-P. Zhu is with the Department of Electrical and Computer Engineering, Concordia University, Montreal, Canada. He is also an Adjunct Professor with the School of Communication and Information Engineering, Nanjing University of Posts and Telecommunications, Nanjing, China (e-mail: weiping@ece.concordia.ca).

TABLE I: The covariance matching criteria (CMC) and the corresponding representative methods.

Category	Formulation	Representative Methods
CMC1	$\left\ \hat{\mathbf{R}} - \mathbf{R} \right\ _F^2$	ITAM [19], method in [24]
CMC2	$\left\ \hat{\mathbf{R}}^{-\frac{1}{2}} (\hat{\mathbf{R}} - \mathbf{R}) \hat{\mathbf{R}}^{-\frac{1}{2}} \right\ _F^2$	COMET [20], AML [21]
CMC3	$\left\ \mathbf{R}^{-\frac{1}{2}} (\hat{\mathbf{R}} - \mathbf{R}) \mathbf{R}^{-\frac{1}{2}} \right\ _F^2$	SPICE [22], SPA [23]

separation condition limits the estimation precision of ANM. Furthermore, ANM fails to give a satisfying performance in the moderate range of the signal-to-noise ratio (SNR). The structured covariance matrix reconstruction (SCMR), also referred to as the covariance matching technique, is another class of gridless methods [19]–[24], which explores the Hermitian and Toeplitz structural information of the covariance matrix as *a priori*. In particular, the existing covariance matching criteria (CMC) can be divided into three categories as shown in Table I.¹ All these CMC-based methods are statistically consistent in the number of snapshots. In comparison, CMC1 is shown to be inconsistent in SNR since it makes no effort to ensure appropriate subspace approximation while CMC2 and CMC3 yield consistent DOA estimates as the SNR increases. On the other hand, CMC2 exhibits better estimation performance than CMC3 when SNR is low or moderate while CMC3 is applicable to the correlated signals and single-snapshot cases compared to CMC2 [23].

Recently, we have proposed a gridless method for DOA estimation named covariance matrix reconstruction approach (CMRA) based on CMC2 in [25] and [26]. CMRA is applicable to the ULA and SLA and can be regarded as the gridless version of the sparsity-based method. Nevertheless, since CMRA approximates the rank norm by the trace norm, which is a loose approximation of the rank norm, there may exist a large gap between the solutions by using the two norms [27]. Such a difference is similar to that between the ℓ_1 and ℓ_0 norms. In particular, for reconstructing a sparse vector, to promote sparsity to the greatest extent possible, the natural choice of the sparsity metric should be ℓ_0 norm, which, however, is NP-hard to compute. A practical choice of the sparsity metric is the ℓ_1 norm which is a convex relaxation but a loose approximation of the ℓ_0 norm. The gap between the two norms can be mitigated by the nonconvex surrogates, e.g., the ℓ_p ($0 < p < 1$) norm, Logarithm, etc., which are well-studied in literature [28]–[31]. Hence, even though CMRA is able to eliminate the basis mismatch effect and give satisfactory performance in DOA estimation, we believe its ability can be further improved by employing the nonconvex surrogates, which, to the best of our knowledge, have not been studied in literature.

In this paper, motivated by the relationship between the ℓ_1 and ℓ_0 norms, we introduce a family of nonconvex continuous surrogate functions as the sparsity metrics rather than the convex trace norm in CMRA and propose an iteratively

reweighted version of CMRA algorithm, called improved CMRA (ICMRA) to solve the nonconvex problem. Further analysis shows that ICMRA serves as CMRA in the first iteration and a reweighted CMRA in each of the following iterations with the weights being based on the latest estimate. A convergence analysis is also provided to verify that ICMRA is able to obtain at least a suboptimal solution. We then explore the connection between the ICMRA and the sparsity-based methods, as well as the atomic norm, showing that ICMRA is able to enhance the sparsity. Two feasible implementation algorithms are also provided to speed up the convergence. One is to solve its duality problem since by which a faster convergence is observed. The other one gives a closed-form solution by simplifying the constraint. Extensive numerical simulations are carried out to verify the performance of our proposed methods.

Notations used in this paper are as follows. \mathbb{C} denotes the set of complex numbers. For a matrix \mathbf{A} , \mathbf{A}^T , $\bar{\mathbf{A}}$ and \mathbf{A}^H denote the transpose, conjugate and conjugate transpose of \mathbf{A} , respectively. $\|\mathbf{A}\|_F$ denotes the Frobenius norm of \mathbf{A} , $\text{vec}(\mathbf{A})$ denotes the vectorization operator that stacks matrix \mathbf{A} column by column, $\mathbf{A} \odot \mathbf{B}$ is the Khatri-Rao product of matrices \mathbf{A} and \mathbf{B} , and $\text{tr}(\bullet)$ and $\text{rank}(\bullet)$ are the trace and rank operators, respectively. $\mathbf{A} \geq \mathbf{0}$ means that matrix \mathbf{A} is positive semidefinite. $\sigma[\mathbf{A}]$ and $\sigma_i[\mathbf{A}]$ denote the singular value and the i -th singular value of \mathbf{A} , respectively. For a vector \mathbf{x} , $\mathbf{x} \geq \mathbf{0}$ means that every entry of \mathbf{x} is nonnegative, $\|\mathbf{x}\|_2$ denotes the ℓ_2 norm of \mathbf{x} , $\text{diag}(\mathbf{x})$ denotes a diagonal matrix with the diagonal entries being the entries of vector \mathbf{x} in turn. $\text{Re}(\bullet)$ and $\text{Im}(\bullet)$ stand for the real and the imaginary parts of a complex variable, respectively.

The rest of the paper is organized as follows. Section II revisits the signal model, the CMRA method and the atomic norm as the preliminaries. Section III presents a family of nonconvex sparsity metrics and then introduces the ICMRA method. A convergence analysis is also provided at the end of this section. Section IV reveals the relationship between ICMRA and some of the existing methods. Section V provides two feasible implementation algorithms. Simulations are carried out in Section VI to demonstrate the performance of our methods. Finally, Section VII concludes the whole paper.

II. PRELIMINARIES

A. Signal Model

For better illustration, we denote $\Omega = \{\Omega_1, \dots, \Omega_M\} \subseteq \{1, \dots, N\}$ as the sensor index set of a linear array. In particular, the ULA has $\Omega = \{1, \dots, N\}$ and the SLA has $\Omega \subset \{1, \dots, N\}$ with $\Omega_1 = 1$ and $\Omega_M = N$, where M is the number of sensors.² Note that the ULA can be considered as a special case of SLA, hence we use the SLA in the following unless otherwise stated.

Assume K narrowband far-field signals impinge onto an SLA with M sensors from directions of $\boldsymbol{\theta} = \{\theta_1, \dots, \theta_K\}$. The array output with respect to L snapshots is,

$$\mathbf{X}_\Omega = \mathbf{A}_\Omega \mathbf{S} + \mathbf{N}, \quad (1)$$

¹In Table I, $\hat{\mathbf{R}}$ denotes the sample covariance matrix and \mathbf{R} denotes the unknown covariance matrix with a Toeplitz structure to be estimated.

²The SLA considered in this paper only involves the array whose coarray is an N -element ULA.

where $\mathbf{X}_\Omega \in \mathbb{C}^{M \times L}$, $\mathbf{A}_\Omega = [\mathbf{a}_\Omega(\theta_1), \dots, \mathbf{a}_\Omega(\theta_K)] \in \mathbb{C}^{M \times K}$ and $\mathbf{S} \in \mathbb{C}^{K \times L}$ denote the array output, the manifold matrix and the waveform of the impinging signals, respectively. $\mathbf{N} \in \mathbb{C}^{M \times L}$ is the white Gaussian noise with zero mean. The steering vector $\mathbf{a}_\Omega(\theta_k) = [e^{j\pi(\Omega_1-1)\sin\theta_k}, \dots, e^{j\pi(\Omega_M-1)\sin\theta_k}]^T$ contains the DOA information which needs to be determined.

B. The CMRA Method

The CMRA aims to first reconstruct the covariance matrix of the coarray of the SLA according to the output. In particular, let $\mathbf{\Gamma} \in \{0, 1\}^{M \times N}$ be a selection matrix such that the m -th row of $\mathbf{\Gamma}$ contains all zeros but a single 1 at the Ω_m -th position. Then the covariance matrix of \mathbf{X}_Ω can be written as,

$$\begin{aligned} \mathbf{R}_\Omega &= \mathbf{\Gamma}T(\mathbf{u})\mathbf{\Gamma}^T + \sigma\mathbf{I} \\ &= T_\Omega(\mathbf{u}) + \sigma\mathbf{I}, \end{aligned} \quad (2)$$

where σ denotes the noise power and $T_\Omega(\mathbf{u}) \triangleq \mathbf{\Gamma}T(\mathbf{u})\mathbf{\Gamma}^T$ in which $T(\mathbf{u})$ is a Toeplitz Hermitian matrix with $\mathbf{u} = [u_1, \dots, u_N]^T$ being the first column of $T(\mathbf{u})$. In practical applications, \mathbf{R}_Ω is approximated by the sample covariance matrix with L snapshots as,

$$\hat{\mathbf{R}}_\Omega = \frac{1}{L} \mathbf{X}_\Omega \mathbf{X}_\Omega^H. \quad (3)$$

The error between $\hat{\mathbf{R}}_\Omega$ and \mathbf{R}_Ω is defined as $\mathbf{E}_\Omega = \hat{\mathbf{R}}_\Omega - \mathbf{R}_\Omega$ which has the following property,

$$\|\mathbf{Q}\text{vec}(\mathbf{E}_\Omega)\|_2^2 \sim \text{As}\chi^2(M^2), \quad (4)$$

where $\mathbf{Q} = \sqrt{L}\mathbf{R}_\Omega^{-\frac{T}{2}} \otimes \mathbf{R}_\Omega^{-\frac{1}{2}}$, and $\text{As}\chi^2(M^2)$ denotes the asymptotic chi-square distribution with M^2 degrees of freedom (see [25], [32] for more details). As a result, CMRA formulates the following low-rank matrix reconstruction (LRMR) model for $T(\mathbf{u})$,

$$\min_{\mathbf{u}} \text{rank}[T(\mathbf{u})] \quad \text{s.t.} \quad \|\mathbf{Q}\text{vec}(\mathbf{E}_\Omega)\|_2^2 \leq \beta^2, T(\mathbf{u}) \geq \mathbf{0}, \quad (5)$$

which is then relaxed into the following convex optimization model by replacing the rank norm with the nuclear norm, or equivalently, the trace norm for a positive semidefinite (PSD) matrix,

$$\min_{\mathbf{u}} \text{tr}[T(\mathbf{u})] \quad \text{s.t.} \quad \|\mathbf{Q}\text{vec}(\mathbf{E}_\Omega)\|_2^2 \leq \beta^2, T(\mathbf{u}) \geq \mathbf{0}, \quad (6)$$

where β can be easily determined by using the property of the chi-square distribution in (4).³ For simplicity, we assume the noise power σ can be estimated as the smallest eigenvalue of $\hat{\mathbf{R}}_\Omega$.⁴ After obtaining $T(\mathbf{u})$ by solving (6), the DOAs θ can be easily determined by using the subspace-based methods or the Vandermonde decomposition lemma (see [23] for more details).

³In this paper, parameter β in CMRA and the proposed ICMRA is calculated using MATLAB routine `chi2inv(1-p, M^2)`, where p is set to 0.001 in general.

⁴This assumption, which is a compromise due to the lack of knowledge of the number of signals, is reasonable with moderate or large number of snapshots since the error-suppression criterion in (6) can tolerate well this underestimated error [11].

Remark 1: It should be noted that, in the case of using an SLA, if the number of impinging signals is equal to or larger than that of sensors, the space of the impinging signals will exceed the space generated by the array. As a consequence, estimating the noise power as the smallest eigenvalue of $\hat{\mathbf{R}}_\Omega$ is impractical. To handle this special case, we should first reconstruct the whole space spanned by the coarray, where the space of the impinging signals not fully occupy. To do this, the Hermitian Toeplitz structure of the covariance matrix can be used. In particular, let $\hat{\mathbf{R}}^{\text{full}} = \mathbf{\Gamma}^T \hat{\mathbf{R}}_\Omega \mathbf{\Gamma}$ and replace its zero elements with the mean of the nonzero entries in the same diagonals. In this way, the impinging signals will fall into the space spanned by the coarray and the noise power can be obtained as the smallest eigenvalue of $\hat{\mathbf{R}}^{\text{full}}$.

C. Atomic Norm

The concept of atomic norm was first introduced in [16], which generalizes many norms such as ℓ_1 norm and the nuclear norm. Considering the DOA estimation using a ULA, let

$$\mathcal{A} = \left\{ \frac{1}{N} \mathbf{a}(\theta) \mathbf{a}^H(\theta) : \theta \in [-90^\circ, 90^\circ] \right\}, \quad (7)$$

which is a set of unit-norm rank-one matrices. The atomic ℓ_0 norm of $T(\mathbf{u})$ is defined as the smallest number of atoms in \mathcal{A} composing $T(\mathbf{u})$, which is shown as,

$$\begin{aligned} \|T(\mathbf{u})\|_{\mathcal{A},0} &= \inf_{c_k > 0} \left\{ \mathcal{K} : T(\mathbf{u}) = \sum_{k=1}^{\mathcal{K}} c_k \mathbf{B}(\theta_k), \mathbf{B}(\theta_k) \in \mathcal{A} \right\} \\ &= \text{rank}[T(\mathbf{u})]. \end{aligned} \quad (8)$$

Hence, model (5) is equivalent to,

$$\min_{\mathbf{u}} \|T(\mathbf{u})\|_{\mathcal{A},0} \quad \text{s.t.} \quad \|\mathbf{Q}\text{vec}(\mathbf{E})\|_2^2 \leq \beta^2, T(\mathbf{u}) \geq \mathbf{0}. \quad (9)$$

It is easy to see that although the atomic ℓ_0 norm directly enhances sparsity, it is nonconvex and NP-hard to compute. Hence the relaxation of $\|T(\mathbf{u})\|_{\mathcal{A},0}$, named the atomic norm, is introduced as,

$$\begin{aligned} \|T(\mathbf{u})\|_{\mathcal{A}} &= \inf_{c_k > 0} \left\{ \sum_k c_k : T(\mathbf{u}) = \sum_{k=1}^{\mathcal{K}} c_k \mathbf{B}(\theta_k), \mathbf{B}(\theta_k) \in \mathcal{A} \right\} \\ &= \sum_k N p_k \\ &= \text{tr}[T(\mathbf{u})], \end{aligned} \quad (10)$$

which indicates that model (6) is equivalent to

$$\min_{\mathbf{u}} \|T(\mathbf{u})\|_{\mathcal{A}} \quad \text{s.t.} \quad \|\mathbf{Q}\text{vec}(\mathbf{E})\|_2^2 \leq \beta^2, T(\mathbf{u}) \geq \mathbf{0}. \quad (11)$$

It should be mentioned that, the solution obtained by solving (6) or (11) is usually suboptimal to the corresponding LRMR problem since the trace norm is a loose approximation of the rank norm, i.e., there still exists a noticeable gap between the solutions of the two norms. To achieve a better approximation of the rank norm, the next section, we propose an iterative reweighted method by introducing a family of nonconvex penalties as the sparsity metrics rather than the trace norm.

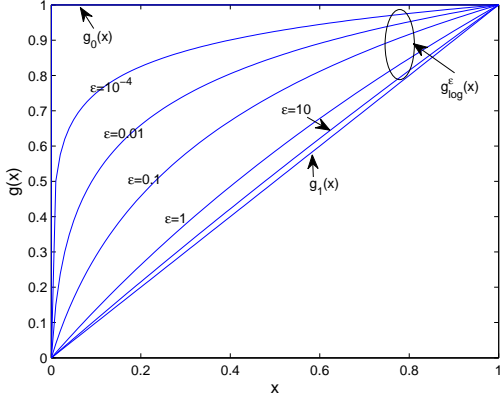


Fig. 1: Illustration of $g_0(x)$, $g_1(x)$ and $g_{\log}^\epsilon(x)$.

III. IMPROVED CMRA

A. The Novel Sparsity Metrics

It is easy to see that the rank norm in model (5) is nonconvex and challenging to solve, while the trace norm, which is utilized in the CMRA method, is computable and the best convex approximation of the rank norm but has the worst fitting. Hence it is essential to find a better approximation of the rank norm but still with a low computational complexity. In particular, for a matrix $\mathbf{X} \in \mathbb{C}^{N \times N}$, the rank and nuclear norm can be represented as

$$\begin{aligned} \text{rank}[\mathbf{X}] &= \min_i \sigma_i(\mathbf{X}) > 0 = \sum_i g_0[\sigma_i(\mathbf{X})]; \\ \|\mathbf{X}\|_* &= \sum_i \sigma_i(\mathbf{X}) = \sum_i g_1[\sigma_i(\mathbf{X})], \end{aligned} \quad (12)$$

respectively, where we have assumed $\sigma_1[\mathbf{X}] \geq \sigma_2[\mathbf{X}] \geq \dots \geq \sigma_N[\mathbf{X}] \geq 0$, and

$$g_0(x) = \begin{cases} 1 & x > 0 \\ 0 & x = 0 \end{cases}; \quad g_1(x) = x, \quad x \geq 0. \quad (13)$$

Hence finding an approximation of the rank norm is equivalent to find a nonconvex sparsity metric $g(x)$ which bridges the gap between $g_0(x)$ and $g_1(x)$ (see Fig. 1). To the best of our knowledge, there exist several nonconvex penalties in literature including Logarithm [29], ℓ_p norm [28] and Laplace [31] which we denote as $g_{\log}^\epsilon(x)$, $g_{\ell_p}^\epsilon(x)$ and $g_{\text{lap}}^\epsilon(x)$, respectively, where ϵ denotes the trade-off parameter. To illustrate these penalties more precisely, we enumerate of them in Table II for comparison and show the curve of $g_{\log}^\epsilon(x)$ with respect to different ϵ as an example in Fig. 1,⁵ from which we can see that $g_{\log}^\epsilon(x)$ approaches $g_1(x)$ with a large value of ϵ and gets close to $g_0(x)$ when $\epsilon \rightarrow 0$. Note that $g_{\ell_p}^\epsilon(x)$ and $g_{\text{lap}}^\epsilon(x)$ have similar properties which are omitted for brevity. In fact, these functions g can be employed as the nonconvex penalties since they satisfy the following properties:

P1: g is concave, monotonically increasing on $[0, +\infty)$.

P2: g is continuous but possibly nonsmooth on $[0, +\infty)$.

⁵ $g_{\log}^\epsilon(x)$ is translated and scaled such that it equals 0 and 1 at $x = 0$ and 1 respectively for better illustration.

TABLE II: Some nonconvex penalties of $g_0(x)$ and their gradients.

Penalty	$g^\epsilon(x), x \geq 0, \epsilon > 0$	gradient $\nabla g^\epsilon(x)$
Logarithm	$\ln(x + \epsilon)$	$\frac{1}{x + \epsilon}$
ℓ_p norm	x^ϵ	$\epsilon x^{\epsilon-1}$
Laplace	$1 - e^{-\frac{x}{\epsilon}}$	$\frac{1}{\epsilon} e^{-\frac{x}{\epsilon}}$

P3: after being translated and scaled, g approaches g_0 when $\epsilon \rightarrow 0$ and g_1 when ϵ is large.

Some other functions satisfying the aforementioned properties have also been proposed as the penalties, e.g., smoothly clipped absolute deviation (SCAD) [33] and minimax concave penalty (MCP) [34], which, however, are omitted in this paper because they usually fail to give a satisfactory performance when employed in an LRMR problem [35].

Motivated by (12), the rank norm model (5) and the trace norm model (6) can be rewritten as,

$$\begin{aligned} \min_{\mathbf{u}} \mathcal{G}[T(\mathbf{u})] \\ \text{s.t. } \|\mathbf{Q}\text{vec}(\mathbf{E}_\Omega)\|_2^2 \leq \beta^2, \quad T(\mathbf{u}) \geq \mathbf{0}, \end{aligned} \quad (14)$$

where $\mathcal{G}[T(\mathbf{u})] = \sum_i g[\sigma_i(T(\mathbf{u}))]$ with $g[\sigma_i(T(\mathbf{u}))]$ being $g_0[\sigma_i(T(\mathbf{u}))]$ for model (5) or $g_1[\sigma_i(T(\mathbf{u}))]$ for model (6).

Further inspired by the link between $g^\epsilon(x)$ and $g_0(x)$ or $g_1(x)$ above, we propose the following general nonconvex optimization model,

$$\begin{aligned} \min_{\mathbf{u}} \mathcal{G}^\epsilon[T(\mathbf{u})] \\ \text{s.t. } \|\mathbf{Q}\text{vec}(\mathbf{E}_\Omega)\|_2^2 \leq \beta^2, \quad T(\mathbf{u}) \geq \mathbf{0}, \end{aligned} \quad (15)$$

where $\mathcal{G}^\epsilon[T(\mathbf{u})] = h^\epsilon[\sigma[T(\mathbf{u})]] = \sum_i g^\epsilon[\sigma_i[T(\mathbf{u})]]$. Intuitively, we expect the new nonconvex model to bridge the gap between models (5) and (6) when ϵ varies from a large number to zero.

B. An Iteratively Reweighted Algorithm

Since model (15) is nonconvex and no efficient algorithms can guarantee to obtain the global minimum, we use the majorization-maximization (MM) method to obtain a suboptimal solution instead. The MM method is an iterative approach and the cost function is replaced by its tangent plane in each iteration. In particular, denote \mathbf{u}_j as the optimization variable of the j -th iteration. Since $\mathcal{G}^\epsilon[T(\mathbf{u})] = \sum_i g^\epsilon[\sigma_i[T(\mathbf{u})]]$ is concave, we have,

$$\mathcal{G}^\epsilon[T(\mathbf{u})] \leq \mathcal{G}^\epsilon[T(\mathbf{u}_j)] + \text{tr}[\nabla \mathcal{G}^\epsilon[T(\mathbf{u}_j)]T(\mathbf{u} - \mathbf{u}_j)], \quad (16)$$

As a result, the optimization problem at the $(j+1)$ -th iteration becomes,

$$\begin{aligned} \min_{\mathbf{u}} \text{tr}[\mathbf{W}_j^\epsilon T(\mathbf{u})] \\ \text{s.t. } \|\mathbf{Q}\text{vec}(\mathbf{E}_\Omega)\|_2^2 \leq \beta^2, \quad T(\mathbf{u}) \geq \mathbf{0}, \end{aligned} \quad (17)$$

where $\mathbf{W}_j^\epsilon \triangleq \nabla \mathcal{G}^\epsilon[T(\mathbf{u}_j)]$. To calculate \mathbf{W}_j^ϵ , we use the following proposition,

Proposition 1 ([36]): Suppose that $\mathcal{G}^\epsilon(\mathbf{X})$ is represented as $\mathcal{G}^\epsilon(\mathbf{X}) = h^\epsilon(\boldsymbol{\sigma}(\mathbf{X})) = \sum_i g^\epsilon(\sigma_i(\mathbf{X}))$, where

$\mathbf{X} \geq \mathbf{0}$ with the singular value decomposition (SVD) $\mathbf{X} = \mathbf{D}\text{diag}[\boldsymbol{\sigma}(\mathbf{X})]\mathbf{D}^T$. Denote two mappings h^ϵ and f^ϵ which are differentiable and concave. Then the gradient of $\mathcal{G}^\epsilon(\mathbf{X})$ at \mathbf{X} is

$$\nabla \mathcal{G}^\epsilon(\mathbf{X}) = \mathbf{D}\text{diag}(\boldsymbol{\eta})\mathbf{D}^T, \quad (18)$$

where $\boldsymbol{\eta} = \nabla h^\epsilon(\boldsymbol{\sigma}(\mathbf{X}))$ denotes the gradient of h at $\boldsymbol{\sigma}(\mathbf{X})$. For simplicity, we denote $\boldsymbol{\sigma}^j = \boldsymbol{\sigma}[T(\mathbf{u}_j)]$. Based on the proposition above, we have,

$$\mathbf{W}_j^\epsilon = \mathbf{U}_j \text{diag}[\nabla h^\epsilon(\boldsymbol{\sigma}^j)] \mathbf{U}_j^H, \quad (19)$$

where $T(\mathbf{u}_j) = \mathbf{U}_j \text{diag}(\boldsymbol{\sigma}^j) \mathbf{U}_j^H$ is the SVD of $T(\mathbf{u}_j)$. It should be noted that, when the Logarithm or the ℓ_p norm penalty is employed, equation (19) can be accelerated as $\mathbf{W}_j^\epsilon = (T(\mathbf{u}_j) + \epsilon \mathbf{I})^{-1}$ or $\mathbf{W}_j^\epsilon = \epsilon [T(\mathbf{u}_j)]^{\epsilon-1}$.

As mentioned before, ϵ controls the relationship between $g^\epsilon(\sigma)$ and $g_0(\sigma)$ or $g_1(\sigma)$. In particular, with a small value of ϵ , $g^\epsilon(\sigma)$ approaches $g_0(\sigma)$ but suffers from many local minima, whereas a large value of ϵ pushes $g^\epsilon(\sigma)$ toward the convex $g_1(\sigma)$, which however has the worst fitting to $g_0(\sigma)$. Consequently, we should start with a large value of ϵ , and gradually decrease it during the iteration to reduce the risk of getting trapped in local minima. Moreover, in each iteration, we also define the weight \mathbf{W}_j^ϵ using the latest solution for avoiding local minima.

After obtaining $T(\mathbf{u})$, similar to CMRA, the DOAs $\boldsymbol{\theta}$ can be easily determined by using the subspace-based methods or the Vandermonde decomposition lemma (see [23] for more details). Before closing this subsection, we summarize the proposed ICMRA in Algorithm 1.

Algorithm 1 ICMRA

Input: measurement data \mathbf{X}_Ω, β .

Initialization: $j = 0, \mathbf{u}_0 = \mathbf{0}, \epsilon$.

repeat

 Update the weight \mathbf{W}_j^ϵ by equation (19);

 Update \mathbf{u}_{j+1} by solving problem (17);

$\epsilon = \frac{\epsilon}{\delta}$ ($\delta > 1$),

$j = j + 1$,

end

until Convergence

Output: $\hat{\boldsymbol{\theta}}$ by using the Vandermonde decomposition lemma.

Remark 2: It should be noted that, when starting with $\mathbf{u}_0 = \mathbf{0}$, the weight $\mathbf{W}_0^\epsilon = c\mathbf{I}$ where c is a positive nonzero constant. Hence the first iteration of ICMRA reduces to the CMRA method. From the second iteration, the weight \mathbf{W}_j^ϵ is determined based on the solution of the previous iteration and thus a reweighted CMRA is carried out in each iteration.

Remark 3: The ICMRA is able to enhance the sparsity and give a better performance than CMRA does, which can be justified as follows.

The problem (17) can be written as (the two constraints in (17) are omitted for brevity),

$$\begin{aligned} & \min_{\mathbf{u}} \text{tr}[\mathbf{W}_j^\epsilon T(\mathbf{u})] \\ & = \min_{p_k, \theta_k} \text{tr}[\mathbf{W}_j^\epsilon \sum_k p_k \mathbf{a}(\theta_k) \mathbf{a}^H(\theta_k)] \\ & = \min_{p_k, \theta_k} \sum_k \mathbf{a}^H(\theta_k) \mathbf{W}_j^\epsilon \mathbf{a}(\theta_k) p_k \\ & = \min_{p_k, \theta_k} \sum_k \omega_k^{-1} p_k \quad \text{s.t.} \quad \omega_k = \frac{1}{\mathbf{a}^H(\theta_k) \mathbf{W}_j^\epsilon \mathbf{a}(\theta_k)}, \end{aligned} \quad (20)$$

where $\mathbf{a}(\theta_k)$ denotes the steering vector of the coarray of the original array with a signal impinging from direction of θ_k . Recall that $\mathbf{W}_j^\epsilon = (T(\mathbf{u}_j) + \epsilon \mathbf{I})^{-1}$ when the Logarithm penalty is used, hence ω_k can be regarded as the power spectrum of the Capon's beamforming if $T(\mathbf{u}_j)$ is interpreted as the covariance matrix of the noiseless array output and ϵ as the noise power. Therefore, the weights $\{\omega_k\}$ lead to finer details of the power spectrum in the current iteration and hence enhance the sparsity [37]. Furthermore, since $g_{\ell_p}^\epsilon(\sigma^j)$ and $g_{\text{lap}}^\epsilon(\sigma^j)$ have similar sparsity enhancing properties to $g_{\text{log}}^\epsilon(\sigma^j)$ as shown in Fig. 1, they can also be used for performance improvement, which will be shown in simulations.

C. Convergence Analysis

In this section, we give the convergence analysis of ICMRA for (15) as the following theorem.

Theorem 1: Denote \mathbf{u}_j as the solution of (17) in the $(j-1)$ -th iteration. Then, the sequence $\{\mathbf{u}_j\}$ satisfies the following properties:

(1) $\mathcal{G}^\epsilon[T(\mathbf{u}_j)]$ is monotonically decreasing and bounded as $j \rightarrow +\infty$.

(2) The sequence $\{\mathbf{u}_j\}$ converges to a local minimum of (15).

Proof 1: Please see Appendix A.

Theorem 1 shows that by iteratively solving (17), we can finally obtain a local minimum of (15).

IV. CONNECTION TO PRIOR ARTS

A. Connection to the sparsity-based methods

We start by extending the last equality of (20) to a convex one by using the sparse representation theory. Suppose that the whole angle space $[-90^\circ, 90^\circ]$ is divided by using a uniform grid of N' points $\boldsymbol{\vartheta}' \triangleq \{\vartheta_1, \dots, \vartheta_{N'}\}$ and further assume that the true DOAs $\boldsymbol{\theta}$ lie exactly on the grid, i.e., $\boldsymbol{\theta} \subset \boldsymbol{\vartheta}'$. Denote the corresponding manifold matrix and power by $\mathbf{A}'_\Omega \in \mathbb{C}^{M \times N'}$ and $\mathbf{p}' = [p_1, \dots, p_{N'}] \in \mathbb{R}^{N' \times 1}$, respectively, and $\tilde{\mathbf{A}}'_\Omega = \tilde{\mathbf{A}}'_\Omega \odot \mathbf{A}'_\Omega$ and $\mathbf{r}_\Omega = \text{vec}(\tilde{\mathbf{R}}_\Omega - \sigma \mathbf{I})$. The resulting sparse model is shown as,

$$\min_{\mathbf{p}' \succeq \mathbf{0}} \sum_n \frac{p_n}{\omega_n^{(j)}} \quad \text{s.t.} \quad \left\| \mathbf{Q}(\mathbf{r}_\Omega - \tilde{\mathbf{A}}'_\Omega \mathbf{p}') \right\|_2^2 \leq \gamma, \quad (21)$$

where $\omega_n^{(j)}$ denotes the n -th weight in the j -th iteration. It is easy to see that model (21) is a reweighted ℓ_1 norm minimization model where the weights $\{\omega_n\}$ are used to enhance the sparsity of the solution and improve the reconstruction performance [38]. In particular, to promote sparsity, ω_n should

be selected such that it has a large value when $p_n \neq 0$ and significantly smaller one elsewhere. With this strategy, after p'_j is determined in the $(j-1)$ -th iteration, the weight $\omega_n^{(j)}$ can be obtained as,

$$\omega_n^{(j)} = \frac{1}{\mathbf{a}^H(\vartheta_n) \mathbf{W}_j^\epsilon \mathbf{a}(\vartheta_n)}, \quad (22)$$

where \mathbf{W}_j^ϵ can be computed by (19) and the estimated covariance $T(\mathbf{u}_j)$ of (19) in each iteration is obtained as $T(\mathbf{u}_j) = \sum_n p_n^{(j)} \mathbf{a}(\vartheta_n) \mathbf{a}^H(\vartheta_n)$. $\{\omega_n\}$ can be regarded as the power spectrum of the Capon's beamforming, which satisfies the selection condition of ω_n as shown in Section III-B. By comparing the sparsity-based model (21) with (20), it can be easily concluded that model (17) is equivalent to (21) with $N' \rightarrow \infty$. In other words, the sparsity-based method (21) is a discretized version of model (17). Finally, it is interesting to note that when $\mathbf{W}_j^\epsilon = \mathbf{I}$, i.e., $\omega_n = \frac{1}{N}$, model (21) is the sparsity-based model proposed in [26]. It should be noted that since the weights $\{\omega_n\}$ enhance the sparsity, the reweighted ℓ_1 norm iterative model (21) is expected to be superior to the ℓ_1 norm model in [26].

B. Connection to Atomic Norm

In this section, we attempt to interpret (17) as an ANM method. To do this, let us first define a weighted continuous dictionary,

$$\mathcal{A}^\omega = \{ \mathbf{B}^\omega(\theta) \} = \left\{ \frac{1}{N} \omega(\theta) \mathbf{a}(\theta) \mathbf{a}^H(\theta) : \theta \in [-90^\circ, 90^\circ] \right\}, \quad (23)$$

where $\omega(\theta) \geq 0$ is a weighting function. Based on (23), the weighted atomic norm of $T(\mathbf{u})$ is defined as,

$$\begin{aligned} & \|T(\mathbf{u})\|_{\mathcal{A}^\omega} \\ &= \inf \left\{ \sum_k c_k^\omega : T(\mathbf{u}) = \sum_k c_k^\omega \mathbf{B}^\omega(\theta_k), \mathbf{B}^\omega(\theta) \in \mathcal{A}^\omega \right\} \\ &= \inf \left\{ \sum_k c_k^\omega : T(\mathbf{u}) = \sum_k c_k^\omega \omega(\theta_k) \mathbf{B}(\theta_k), \mathbf{B}(\theta) \in \mathcal{A} \right\} \\ &= \inf \left\{ \sum_k c_k \omega^{-1}(\theta_k) : T(\mathbf{u}) = \sum_k c_k \mathbf{B}(\theta_k), \mathbf{B}(\theta_k) \in \mathcal{A} \right\} \\ &= \sum_k N \omega_k^{-1} p_k \\ &= N \text{tr}[\mathbf{W}^\epsilon T(\mathbf{u})], \end{aligned} \quad (24)$$

which indicates that model (17) is equivalent to the following ANM model,

$$\begin{aligned} & \min_{\mathbf{u}} \|T(\mathbf{u})\|_{\mathcal{A}^\omega} \\ & \text{s.t. } \|\mathbf{Q} \text{vec}(\mathbf{E}_\Omega)\|_2^2 \leq \beta^2, \quad T(\mathbf{u}) \geq \mathbf{0}. \end{aligned} \quad (25)$$

According to the third equation in (24), an atom $\mathbf{B}(\theta)$, $\theta \in [-90^\circ, 90^\circ]$, is selected with a high probability if $\omega(\theta)$ is larger, which is the same conclusion as shown in Section IV-A.

V. COMPUTATIONALLY EFFICIENT IMPLEMENTATIONS

Here we present two implementation algorithms to speed up the convergence of the proposed method.

A. Optimization via Duality

We have empirically observed that a faster speed can be achieved when we solve the dual problem of model (17) as shown in the following.

First, by using the substitution $\mathbf{Y} = T(\mathbf{u})$, problem (17) can be reformulated as,

$$\begin{aligned} & \min_{\mathbf{u}, \mathbf{Y}} \text{tr}[\mathbf{W}_j^\epsilon \mathbf{Y}] \\ & \text{s.t. } \mathbf{Y} - T(\mathbf{u}) = \mathbf{0}, \\ & \quad T(\mathbf{u}) \geq \mathbf{0}, \\ & \quad \left\| \mathbf{Q} \text{vec}(\hat{\mathbf{R}}_{-\sigma} - \mathbf{Y}_\Omega) \right\|_2^2 \leq \beta^2, \end{aligned} \quad (26)$$

where $\hat{\mathbf{R}}_{-\sigma} = \hat{\mathbf{R}}_\Omega - \sigma \mathbf{I}$, $\mathbf{Y}_\Omega = \mathbf{\Gamma} \mathbf{Y} \mathbf{\Gamma}^T$. Let $\mathbf{\Lambda}$, \mathbf{V} and μ be the Lagrangian multipliers of the three constraints of (26), respectively. We can obtain the Lagrangian associated with the problem (26) as,

$$\begin{aligned} & \mathcal{L}(\mathbf{u}, \mathbf{Y}, \mathbf{\Lambda}, \mathbf{V}, \mu) \\ &= \text{tr}[\mathbf{W}_j^\epsilon \mathbf{Y}] - \text{tr}[\mathbf{\Lambda}(\mathbf{Y} - T(\mathbf{u}))] - \text{tr}[\mathbf{V}T(\mathbf{u})] \\ & \quad + \mu \left\| \mathbf{Q} \text{vec}(\hat{\mathbf{R}}_{-\sigma} - \mathbf{Y}_\Omega) \right\|_2^2 - \mu \beta^2 \\ &= \text{tr}[(\mathbf{W}_{j\Omega}^\epsilon - \mathbf{\Lambda}_\Omega) \mathbf{Y}_\Omega] + (\omega_{\bar{\Omega}} - \lambda_{\bar{\Omega}})^H \mathbf{y}_{\bar{\Omega}} \\ & \quad + \text{tr}[(\mathbf{\Lambda} - \mathbf{V})T(\mathbf{u})] + \mu \left\| \mathbf{Q} \text{vec}(\hat{\mathbf{R}}_{-\sigma} - \mathbf{Y}_\Omega) \right\|_2^2 - \mu \beta^2, \end{aligned} \quad (27)$$

where $\mathbf{W}_{j\Omega}^\epsilon = \mathbf{\Gamma} \mathbf{W}_j^\epsilon \mathbf{\Gamma}^T$ and $\mathbf{\Lambda}_\Omega = \mathbf{\Gamma} \mathbf{\Lambda} \mathbf{\Gamma}^T$. Also, $\omega_{\bar{\Omega}}$, $\lambda_{\bar{\Omega}}$ and $\mathbf{y}_{\bar{\Omega}}$ are the vectors composed of the entries of $\mathbf{W}_{j\Omega}^\epsilon$, $\mathbf{\Lambda}$ and \mathbf{Y} , whose rows and columns are indexed by $\bar{\Omega}$, respectively, in which $\bar{\Omega} = \{1, \dots, N\} - \Omega$. Then, the Lagrange dual with respect to (26) can be easily formulated as follows,

$$\begin{aligned} \mathcal{G} &= \min_{\mathbf{u}, \mathbf{Y}} \max_{\mathbf{\Lambda}, \mathbf{V}, \mu} \mathcal{L}(\mathbf{u}, \mathbf{Y}, \mathbf{\Lambda}, \mathbf{V}, \mu) \\ &= \max_{\mathbf{\Lambda}, \mathbf{V}, \mu} \min_{\mathbf{u}, \mathbf{Y}} \mathcal{L}(\mathbf{u}, \mathbf{Y}, \mathbf{\Lambda}, \mathbf{V}, \mu) \\ &= \max_{\mathbf{\Lambda}, \mathbf{V}, \mu} -\frac{1}{4\mu} \left\| \mathbf{Q}^{-H} \text{vec}(\mathbf{W}_{j\Omega}^\epsilon - \mathbf{\Lambda}_\Omega) \right\|_2^2 - \mu \beta^2 \\ & \quad + \text{vec}(\hat{\mathbf{R}}_{-\sigma})^H \text{vec}(\mathbf{W}_{j\Omega}^\epsilon - \mathbf{\Lambda}_\Omega) \\ & \text{s.t. } \begin{cases} \mathbf{V} \geq \mathbf{0}, \\ T^*(\mathbf{\Lambda} - \mathbf{V}) = \mathbf{0}, \\ \lambda_{\bar{\Omega}} = \omega_{\bar{\Omega}}, \end{cases} \end{aligned} \quad (28)$$

where $T^*(\mathbf{V}) = [v_{-(N-1)}, \dots, v_{N-1}]^T$, with v_n being the sum of the n -th diagonal of $\mathbf{V} \in \mathbb{C}^{N \times N}$. The second equality in (28) holds because of strong duality [39]. Then by noting that $\frac{1}{4\mu} \left\| \mathbf{Q}^{-H} \text{vec}(\mathbf{W}_{j\Omega}^\epsilon - \mathbf{\Lambda}_\Omega) \right\|_2^2 + \mu \beta^2 \geq \beta \left\| \mathbf{Q}^{-H} \text{vec}(\mathbf{W}_{j\Omega}^\epsilon - \mathbf{\Lambda}_\Omega) \right\|_2$, the dual problem of (26) can be formulated as,

$$\begin{aligned} & \min_{\mathbf{\Lambda}, \mathbf{V}} \beta \left\| \mathbf{Q}^{-H} \text{vec}(\mathbf{W}_{j\Omega}^\epsilon - \mathbf{\Lambda}_\Omega) \right\|_2 \\ & \quad - \text{vec}(\hat{\mathbf{R}}_{-\sigma})^H \text{vec}(\mathbf{W}_{j\Omega}^\epsilon - \mathbf{\Lambda}_\Omega) \\ & \text{s.t. } \begin{cases} \mathbf{V} \geq \mathbf{0}, \\ T^*(\mathbf{\Lambda} - \mathbf{V}) = \mathbf{0}, \\ \lambda_{\bar{\Omega}} = \omega_{\bar{\Omega}}, \end{cases} \end{aligned} \quad (29)$$

which is also convex and can be solved using CVX. Since the strong duality holds, the solution to problem (17) can be obtained as the dual variable of \mathbf{V} . As a result, the reweighted algorithm can be iteratively implemented and the DOAs can be estimated.

B. A Fast Implementation for ICMRA

Although solving the dual problem can save computations to some extent, the employed CVX solver is still time-consuming. In this section, we propose a computationally efficient method by deriving a closed-form solution.

In our model (17), the covariance matrix $T(\mathbf{u})$ is constrained to be positive semidefinite, which is almost sure with moderate or large number of snapshots. The research in [21] indicates that $L \geq 15$ is large enough to ensure that the estimated covariance matrix is positive semidefinite in a 5-element ULA case. Here we focus on moderate/large values of L , and thus drop the constraint $T(\mathbf{u}) \geq \mathbf{0}$ in (17) for speed consideration and rewrite it into the Lagrangian form below,

$$\min_{\mathbf{u}} \lambda \text{tr}[\mathbf{W}_j^\epsilon T(\mathbf{u})] + \frac{1}{2} \left\| \mathbf{Q} \text{vec}(\hat{\mathbf{R}}_{-\sigma} - T_\Omega(\mathbf{u})) \right\|_2^2, \quad (30)$$

where $\lambda > 0$ is a lagrangian multiplier. We then rewrite (30) as,

$$\begin{aligned} & \min_{\mathbf{u}} \lambda \text{tr}[\mathbf{W}_j^\epsilon T(\mathbf{u})] + \frac{1}{2} \left\| \mathbf{Q} \text{vec}(\hat{\mathbf{R}}_{-\sigma} - T_\Omega(\mathbf{u})) \right\|_2^2 \\ &= \min_{\mathbf{u}} \lambda \text{tr}[\mathbf{W}_j^\epsilon T(\mathbf{u})] + \frac{1}{2} \left[\text{vec}^H(\hat{\mathbf{R}}_{-\sigma} - T_\Omega(\mathbf{u})) \right. \\ & \quad \left. \times \text{vec}(\hat{\mathbf{R}}_{-\sigma}^{-1}(\hat{\mathbf{R}}_{-\sigma} - T_\Omega(\mathbf{u}))\hat{\mathbf{R}}_{-\sigma}^{-1}) \right] \\ &= \min_{\mathbf{u}} \lambda \text{tr}[\mathbf{W}_j^\epsilon T(\mathbf{u})] + \frac{1}{2} \left[\text{tr}[T_\Omega(\mathbf{u})\hat{\mathbf{R}}_{-\sigma}^{-1}T_\Omega(\mathbf{u})\hat{\mathbf{R}}_{-\sigma}^{-1}] \right. \\ & \quad \left. - 2\text{tr}[T_\Omega(\mathbf{u})\hat{\mathbf{R}}_{-\sigma}] \right] \\ &= \min_{\mathbf{u}} \text{tr}[(\lambda \mathbf{W}_j^\epsilon - \mathbf{C})T(\mathbf{u})] + \frac{1}{2} \text{tr}[T(\mathbf{u})CT(\mathbf{u})\mathbf{C}], \end{aligned} \quad (31)$$

where $\mathbf{C} = \mathbf{\Gamma}^T \hat{\mathbf{R}}_{-\sigma}^{-1} \mathbf{\Gamma}$. By letting the derivative of the last objective function in (31) with respect to \mathbf{u} be zero, it can be shown that the optimal solution of (31) satisfies the following equality,

$$T^*(\mathbf{C} - \lambda \mathbf{W}_j^\epsilon) = T^*(CT(\mathbf{u})\mathbf{C}). \quad (32)$$

Clearly, (32) is an N -variate linear equation which can be solved by the following procedure. First, the right-hand term of (32) can be transformed as,

$$T^*(CT(\mathbf{u})\mathbf{C}) = \underbrace{\begin{bmatrix} \hat{\Phi}_{-1} \\ \Phi \end{bmatrix}}_{\mathbf{Z}} \begin{bmatrix} \mathbf{u}_{-1} \\ \bar{\mathbf{u}} \end{bmatrix}, \quad (33)$$

where

$$\hat{\Phi}_{-1} = [\hat{\Phi}_{N,:}^T, \dots, \hat{\Phi}_{2,:}^T]^T, \quad (34)$$

$$\mathbf{u}_{-1} = [u_N, \dots, u_2]^T, \quad (35)$$

and

$$\Phi = \begin{bmatrix} T^{*T}(\mathbf{C}_{:, \{1, \dots, N\}} \mathbf{C}_{\{1, \dots, N\}, :}) \\ T^{*T}(\mathbf{C}_{:, \{1, \dots, N-1\}} \mathbf{C}_{\{2, \dots, N\}, :}) \\ \vdots \\ T^{*T}(\mathbf{C}_{:, 1} \mathbf{C}_{N, :}) \end{bmatrix}, \quad (36)$$

with $\mathbf{C}_{:, \mathcal{A}}$ and $\mathbf{C}_{\mathcal{B}, :}$ denoting the columns and rows of matrix \mathbf{C} indexed by sets \mathcal{A} and \mathcal{B} , respectively. Then, by letting

$$\mathbf{Z}_1 = f(\mathbf{Z}_{:, \{1:N\}}), \quad (37)$$

and

$$\mathbf{Z}_2 = [\mathbf{0}, \mathbf{Z}_{:, \{N+1:2N-1\}}], \quad (38)$$

where the operator $f(\mathbf{Z})$ returns \mathbf{Z} with row preserved and columns flipped in the left/right direction, we can rewrite (33) into a more compact form,

$$T^*(CT(\mathbf{u})\mathbf{C}) = [\mathbf{Z}_1 \ \mathbf{Z}_2] \begin{bmatrix} \mathbf{u} \\ \bar{\mathbf{u}} \end{bmatrix}. \quad (39)$$

To obtain the estimate \mathbf{u} which is complex-valued, we first transform (39) into a real-valued matrix form as follows,

$$\underbrace{\begin{bmatrix} \text{Re}(\mathbf{h}) \\ \text{Im}(\mathbf{h}) \end{bmatrix}}_{\mathbf{h}_r} = \underbrace{\begin{bmatrix} \text{Re}(\mathbf{Z}_1 + \mathbf{Z}_2) & \text{Im}(\mathbf{Z}_2 - \mathbf{Z}_1) \\ \text{Im}(\mathbf{Z}_1 + \mathbf{Z}_2) & \text{Re}(\mathbf{Z}_1 - \mathbf{Z}_2) \end{bmatrix}}_{\mathbf{Z}_r} \underbrace{\begin{bmatrix} \text{Re}(\mathbf{u}) \\ \text{Im}(\mathbf{u}) \end{bmatrix}}_{\mathbf{u}_r}, \quad (40)$$

where \mathbf{h} denotes the left-hand term of (32) and the subscript r denotes that the variable is real-valued. It is seen from (40) that \mathbf{u} can be easily obtained from $\mathbf{u}_r = \mathbf{Z}_r^\dagger \mathbf{h}_r$, where \dagger is the pseudo-inverse operator. Compared to using CVX, the derived closed-form solution can reduce the computational complexity to a great extent and hence the method is termed as fast ICMRA (FICMRA). Its performance and superiorities over other methods will be shown in the following section.

VI. SIMULATION RESULTS

In this section, we evaluate the performance of (F)ICMRA with comparison to CMRA [26], MUSIC [40], ℓ_1 singular value decomposition (L1-SVD) [7] and sparse and parametric approach (SPA) [23]. In our simulations, ICMRAs are implemented by solving the dual problem as discussed in Section V-A and FICMRAs are carried out by the closed-form solution as derived in Section V-B. We especially consider the closely adjacent signal cases which require high resolution. The nonconvex penalties employed in ICMRA are Logarithm, ℓ_p norm and Laplace and the corresponding proposed methods are (F)ICMRA_{log}, (F)ICMRA _{ℓ_p} and (F)ICMRA_{lap}. For the initialization of ICMRA, we set $\mathbf{u}_0 = \mathbf{0}$ and $\epsilon_0 = 1$, hence the first iteration of ICMRA is equivalent to CMRA. It is expected that other initializations may lead to different estimate $\hat{\mathbf{u}}$. From this point of view, we carry out an empirical analysis of initialization impact on the solution in Section VI-D, and show that starting with a zero vector is an appropriate attempt. For the proposed methods, at each iteration, unless otherwise stated, the value of ϵ is reduced by $\epsilon_{j+1} = \frac{\epsilon_j}{\delta}$ with $\delta = 2, 10, 10$ for Logarithm, ℓ_p and Laplace, respectively (the choice of δ will be discussed in Section VI-A). The iteration stops if the maximum number of iterations, set to 20, is reached, or

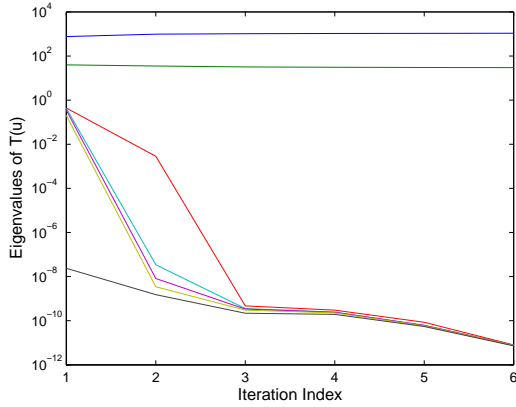


Fig. 2: The variation of eigenvalues of $T(\mathbf{u})$ with respect to the iteration index. The number of snapshots is set to 200 and SNR= 20dB.

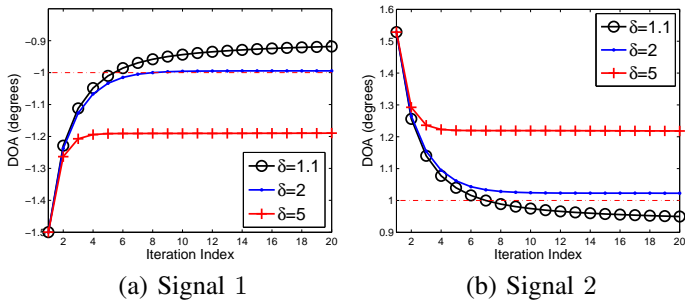


Fig. 3: Iteration results of ICMRA_{\log} .

the relative change of $\hat{\mathbf{u}}$ at two consecutive iterations is less than 10^{-4} , i.e., $\frac{\|\hat{\mathbf{u}}_{j+1} - \hat{\mathbf{u}}_j\|_F}{\|\hat{\mathbf{u}}_j\|_F} < 10^{-4}$. The number of sources is assumed to be unknown for the compared methods except MUSIC. The searching step of MUSIC is determined by the SNR, i.e., $(10^{-\frac{\text{SNR}}{20}} - 1)^\circ$. For the initialization of the three FICMRAs, λ is set to 0.1 which gives good performance empirically. Other settings of FICMRAs are the same as those of the corresponding ICMRAs.

A. An illustration Example

We first carry out a simple example to illustrate the iterative process and choose ICMRA_{\log} as the representative method. Assume two narrowband far-field signals impinge onto a 7-element ULA from directions of $[-1^\circ, 1^\circ]$. Two hundred snapshots are collected for DOA estimation and the SNR is set to 20dB. To illustrate that our iterative procedure is able to promote the sparsity structure, we record the variation of eigenvalues of $T(\mathbf{u}_j)$ with respect to the iteration index and plot them in Fig. 2, in which different color curves denote different eigenvalues. Note that ICMRA is terminated after 10 iterations and we only plot the eigenvalues of the first 6 iterations for better visual effects. From Fig. 2 it can be seen that after the first iteration (a.k.a. the CMRA method), there exist two large eigenvalues, four moderate eigenvalues and only one extremely small eigenvalue. In other words, the

estimated covariance matrix is singular but has at least rank-six. Subsequently, the moderate eigenvalues gradually decrease and approach zero (within numerical precision) after the third iteration while the other two large eigenvalues nearly remain unchanged. Hence by noting that the final covariance matrix estimated by ICMRA has a rank of two, which is equivalent to the number of signals, it can be concluded that the sparse structure is promoted. The ICMRA with two other penalties show similar performance and the details are omitted here.

Next, we discuss the choice of δ and evaluate the influence of different values of δ on estimation performance. In particular, we repeat the previous simulation with $\delta = 1.1, 2, 5$ and show the DOA estimates with respect to each iteration in Fig. 3. The iterations start from CMRA and are able to provide more accurate estimates. Moreover, it can be observed that $\delta = 5$ may lead to a faster convergence speed but subject to a worse estimate (more experiments indicate a larger δ , e.g., $\delta = 10$, may result in some outliers). Among the three choices of δ , it is interesting to note that $\delta = 1.1$ has the slowest convergence speed whereas does not produce the best estimates. In contrast, $\delta = 2$ shows the best estimation performance compared to other choices of δ . Hence $\delta = 2$ is a proper choice for ICMRA_{\log} in terms of both accuracy and speed convergence. The choices of δ for other proposed methods as shown above have also been empirically and carefully determined. In computational speed, for each trial, CMRA (a.k.a. the first iteration of ICMRA_{\log}) takes 0.25s on average while ICMRA_{\log} requires 5.97s because of the iterative procedure. In conclusion, compared to the CMRA, the reweighted iteration strategy is able to improve the resolution at the cost of more expensive computations.

B. DOA Estimation Performance

We now evaluate the DOA estimation performance of the proposed methods with comparison to CMRA. Assume two narrowband signals impinge onto a 7-element ULA from directions of $[-1^\circ, 3^\circ]$. We collect $L = 400$ snapshots which are corrupted by i.i.d. Gaussian noise of unit variance with SNR = 10dB. We show the DOA estimation results of the compared methods in Fig. 4. The powers can be estimated by solving a least squares problem given the corresponding DOA estimates. It can be seen that the outputs of CMRA are biased while the proposed methods ICMRAs/FICMRAs are able to locate the spatially adjacent sources with a higher precision. It is interesting to note that the two sources tend to merge together for all of these methods. It is because the two DOAs are very closely-located. Specifically, when the noise is heavier, or the number of snapshots is smaller, or the sources become closer, we will find that the two red point paths completely merge together, which indicates that we can detect only one single source at this region in some cases. More simulations show that with a higher SNR, larger L and separation, the two paths tend to be parallel, which means the DOAs are estimated with a higher precision. Finally, the running times of each method are compared in Table III. It can be seen that the ICMRAs require the most computations as expected. Note that the CPU times of ICMRA_{\log} and

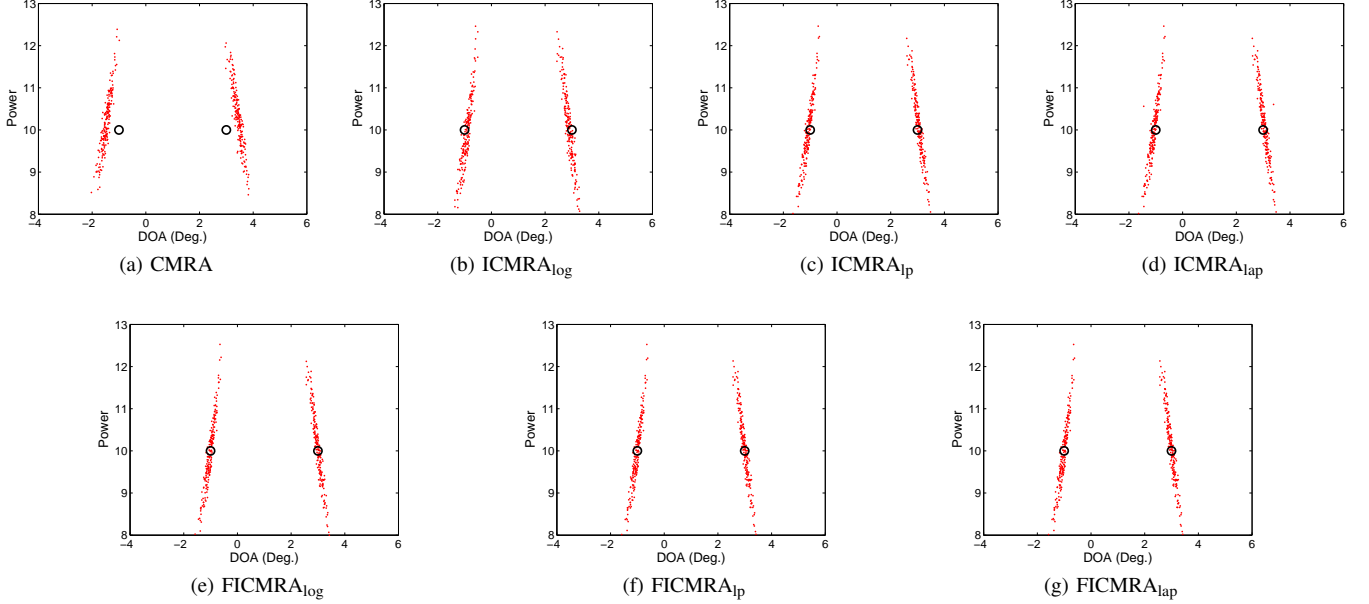


Fig. 4: DOA estimation comparison of CMRA, ICMRA and FICMRA for two uncorrelated sources impinging from $[-1^\circ, 3^\circ]$ with $L = 400$ and $\text{SNR} = 10\text{dB}$.

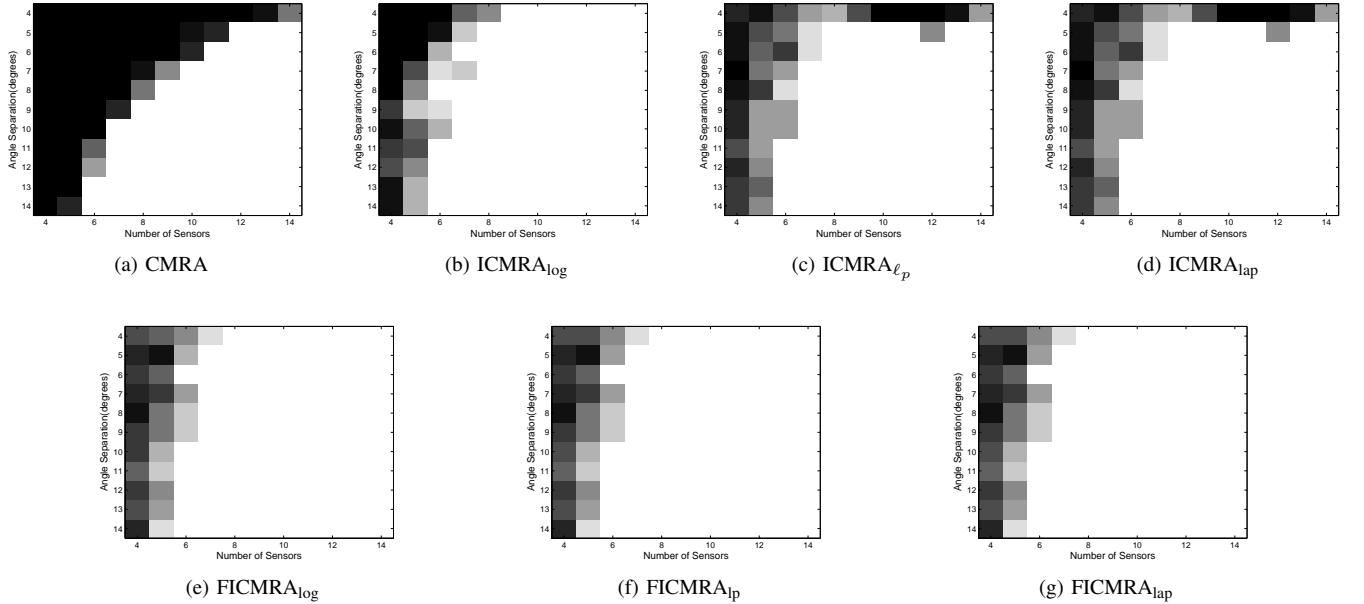


Fig. 5: Success rates of CMRA ICMRA and FICMRA with $L = 400$, $\text{SNR} = 10\text{dB}$.

TABLE III: CPU Time (in seconds) comparison of CMRA and the proposed methods.

	CMRA	ICMRA _{log}	ICMRA _{ℓ_p}	ICMRA _{lap}	FICMRA _{log}	FICMRA _{ℓ_p}	FICMRA _{lap}
CPU Time	0.1670	5.4725	4.6653	2.1171	0.0071	0.0071	0.0033

ICMRA_{ℓ_p} are more than 20 (i.e., the maximum number of iterations) times larger than that of CMRA. This is because the ICMRA involves an additional SVD in each iteration, which is also time-consuming. As mentioned in Section III-B, ICMRA_{log} and ICMRA_{ℓ_p} can be accelerated since the SVD

is not required. Finally, it can be observed that the FICMRAs are computationally very efficient as compared to ICMRAs as well as CMRA.

Next, we study the success rates of ICMRAs, FICMRAs and CMRA in terms of the angle separation $\Delta\theta$ and the number

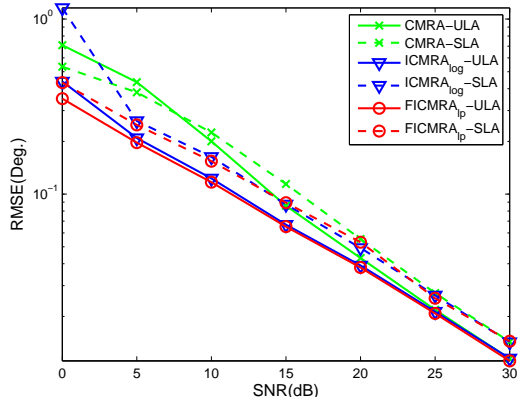


Fig. 6: RMSE results of CMRA, ICMRA_{\log} and FICMRA_{ℓ_p} in the cases of a 7-element ULA and a 4-element SLA with $\Omega = \{1, 2, 5, 7\}$. The signals impinge onto the arrays from directions of $[-5^\circ, 5^\circ]$, $L = 200$.

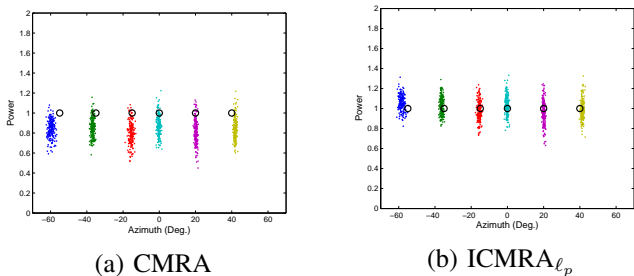


Fig. 7: DOA estimation comparisons of CMRA, ICMRA_{ℓ_p} with more sources than sensors.

of sensors M . It is assumed that two signals impinge onto an M -element ULA from directions of $[-1^\circ, -1^\circ + \Delta\theta]$ where $\Delta\theta$ varies from 4° to 14° and the number of sensors increases from 4 to 14. Successful estimate is declared if the root mean square error (RMSE) of DOA estimation is less than 0.1. The success rates for each pair of M and $\Delta\theta$ are presented based on 50 independent trials in Fig. 5 where white means complete success and black means complete failure. It can be seen that a large value of M or $\Delta\theta$ leads to a high success rate while a small value of M or $\Delta\theta$ may result in unsatisfactory estimates, leading to a phase transition in the M - $\Delta\theta$ domain. By comparing Fig. 5(a)-(g), we can see that ICMRAs/FICMRAs with the three penalties enlarge the success region compared to CMRA. In particular, by noting the fact that ICMRA_{\log} is able to correctly locate the signals separated by $\Delta\theta = 4^\circ$ with a 9-element ULA where ICMRA_{ℓ_p} and $\text{ICMRA}_{\text{lap}}$ fail, it can be concluded that the Logarithm penalty is superior to the ℓ_p and Laplace penalties. Furthermore, Fig. 5(b)-(g) also show that the performance improvement has mostly appeared in the small $\Delta\theta$ s region, demonstrating the ability of our methods in enhancing resolution.

We then consider the estimation performance of the proposed methods in a 4-element SLA case with $\Omega = \{1, 2, 5, 7\}$, as well as a ULA case with the same aperture size, i.e., a 7-

element ULA. Assume two uncorrelated sources impinge onto both arrays from directions of $[-5^\circ, 5^\circ]$ and 200 snapshots are collected, simultaneously. We run 400 independent trials and show the RMSE of CMRA and our methods with the SNR varying from 0dB to 30dB in Fig. 6. For brevity, in this example, we only consider the ICMRA_{\log} and FICMRA_{ℓ_p} as the two representative methods of ICMRA and FICMRA, respectively. From Fig. 6 it can be seen that our proposed methods give a better performance than CMRA in both ULA and SLA cases with respect to most compared region. Furthermore, it should be noted that, compared to the ULA case, the SLA case is able to save 43% data with only a small degradation of 1dB to 1.5dB in terms of RMSE for the three methods when $\text{SNR} \geq 5\text{dB}$. Finally, it can be seen that for each array, the curves of the three methods tend to merge together when SNR is larger than 25dB.

We finally evaluate the performance of our methods in the SLA case with more sources than sensors. In particular, assume six uncorrelated sources impinge onto a 4-element SLA with $\Omega = \{1, 2, 5, 7\}$ from directions of $[-55^\circ, -35^\circ, -15^\circ, 0^\circ, 20^\circ, 40^\circ]$ simultaneously. 400 snapshots which are corrupted by i.i.d. Gaussian noise are collected for source localization and the SNR is set to 0dB. We compare the estimation performance of CMRA and ICMRA_{ℓ_p} via 200 independent trials and show the results in Fig. 7, from which it can be seen that both methods can correctly locate all the 6 sources while ICMRA_{ℓ_p} is able to show better performance in terms of both DOAs and powers. To be specific, the average RMSEs of CMRA with respect to DOA and power are 0.6395 and 0.1828, respectively, while those of ICMRA_{ℓ_p} are 0.5486 and 0.1331, respectively. We have also carried out this experiment on a 4-element SLA using the Logarithm and Laplace penalties, where the Logarithm penalty failed to provide a satisfactory performance in all trials since several outliers are observed in the experiment, especially when the number of sources is equal to or larger than that of sensors. In contrast, the proposed method with the Laplace penalty is able to give a good performance. Here, we report this observation and suggest to use (F)ICMRA $_{\ell_p}$ or (F)ICMRA $_{\text{lap}}$ in the SLA case with the number of sources being larger than that of sensors and use (F)ICMRA $_{\log}$ in other cases.

C. Comparisons with Prior Arts

In this section, the performance of the proposed methods (F)ICMRA with the Logarithm penalty is studied with comparison to other existing methods. The prior arts considered in this part are CMRA, MUSIC, L1-SVD and SPA. For the sparsity-based method L1-SVD, the discretized interval is set to 2° and the iterative grid refinement procedure is employed [7]. In L1-SVD the number of iterations to refine the grid is set to 5 and the grid interval of the last iteration is set to $0.1 \times 10^{-\frac{\text{SNR}}{20}}$ for accuracy consideration. As a consequence, the RMSE of L1-SVD can achieve the Crammer-Rao Lower Bound (CRLB) theoretically.

Suppose that two uncorrelated signals impinge onto a 7-element ULA from $[-1^\circ + v, 3^\circ + v]$ where v is chosen randomly and uniformly within $[-1^\circ, 1^\circ]$ in each trial. Note

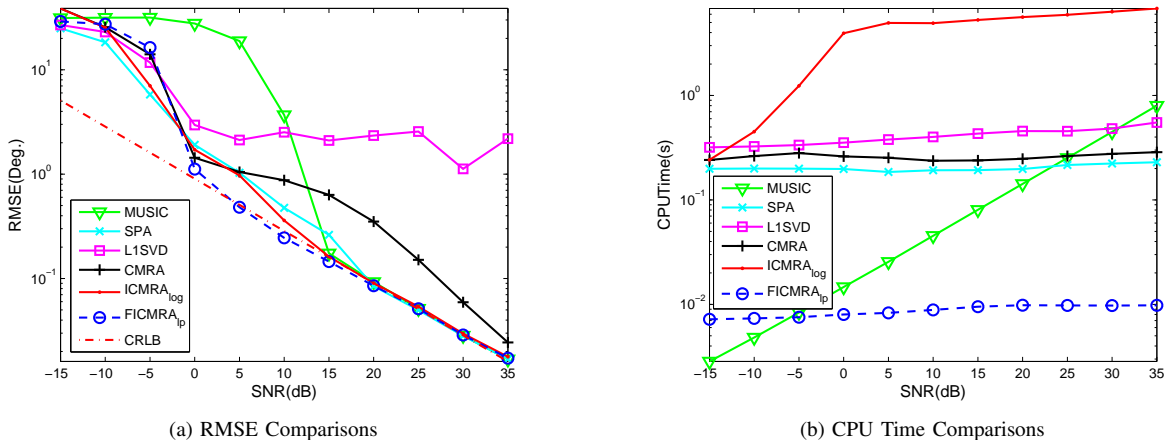


Fig. 8: Performance comparison of ICMRA_{log}, FICMRA_{log} and other methods for two uncorrelated sources impinging from $[-1^\circ + v, 3^\circ + v]$ with the SNR varying from -15 dB to 35 dB, $L = 200$.

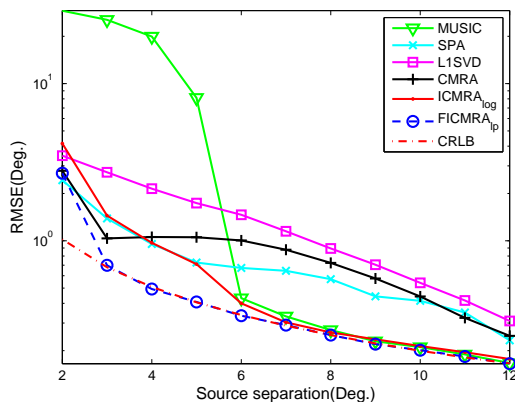


Fig. 9: Performance comparison of ICMRA_{log}, FICMRA_{log} and other methods for two uncorrelated sources impinging from $[0^\circ, \Delta\theta]$ with $\Delta\theta$ varying from 2° to 12° . We set SNR= 15 dB and $L = 200$.

that the two sources are spatially adjacent since they are only separated by around 4° . Assume that 200 snapshots are collected in each trial for DOA estimation. We compare the statistical results of the aforementioned methods obtained from 400 independent trials in Fig. 8 with the SNR varying from -15 dB to 35 dB. Fig. 8(a) shows the RMSE comparisons of these methods, from which we can see that FICMRA_{log} gives the best performance when $\text{SNR} \geq 0$ dB and approaches the CRLB curve first. ICMRA_{log} shows a better result than CMRA in most compared region. In particular, the curve of CMRA deviates the CRLB curve in the middle range of SNR (it approaches the CRLB when $\text{SNR} > 40$ dB) while ICMRA_{log} revises this deviation and is able to coincide with the CRLB curve when $\text{SNR} \geq 15$ dB. In comparison, MUSIC and SPA approach the CRLB curve when $\text{SNR} \geq 15$ dB and 20 dB, respectively. L1-SVD is unable to reach the CRLB in this case of closely-located sources (one possible reason may be the high correlation between the columns of the manifold matrix

in the sparsity-based methods [9]). The running times of each method are also compared in Fig. 8(b). ICMRA_{log} is time-consuming because of the iterative procedure. Nevertheless, it should be noted that, the increased computational cost of ICMRA can be regarded as a sacrifice for resolution improvement. The running time of L1-SVD, CMRA and SPA are comparable with each other and nearly remain stable in the compared SNR region. The FICMRA_{log} requires much smaller computations than other methods when $\text{SNR} \geq -5$ dB. It should be noted that the effectiveness of FICMRA_{log} is because of the derived closed-form solution of model (30) rather than at any cost of the performance deterioration. On the contrary, we can observe that, compared to ICMRA_{log}, FICMRA_{log} is able to reduce the RMSE in some extent. Finally, the running time of MUSIC increases exponentially since the sampling grid size grows as the SNR increases.

We then evaluate the RMSE with respect to different source separations $\Delta\theta$. It is assumed two sources impinge onto a 7-element ULA from $[0^\circ, \Delta\theta]$ and 200 snapshots are collected. We set SNR= 15 dB, $L = 200$ and show the RMSEs of these methods with $\Delta\theta$ varying from 2° to 12° in Fig. 9, which reveals the superiority of our proposed methods in separating spatially adjacent signals. It should be mentioned that, for ICMRA_{log} in this simulation, we set $\delta = 1.1$ as an initial value when $\Delta\theta$ starts from 2° and gradually increase δ until 2 with step 0.1 as $\Delta\theta$ increases. From Fig. 9 it can be observed that our proposed methods outperform other methods in most cases. In particular, FICMRA_{log} is able to coincide with the CRLB when the sources are only 3° apart. ICMRA_{log} and MUSIC approach the CRLB when the source separation is larger than 6° . Note that when $3^\circ < \Delta\theta < 6^\circ$, ICMRA_{log} still can identify the two adjacent sources while MUSIC fails to do so. In contrast, L1-SVD, CMRA and SPA are far from the CRLB in the compared region.

D. Influence of Initialization

In the above simulations we have set $\mathbf{u}_0 = \mathbf{0}$ so that the first iteration is equivalent to the CMRA method. The simulation

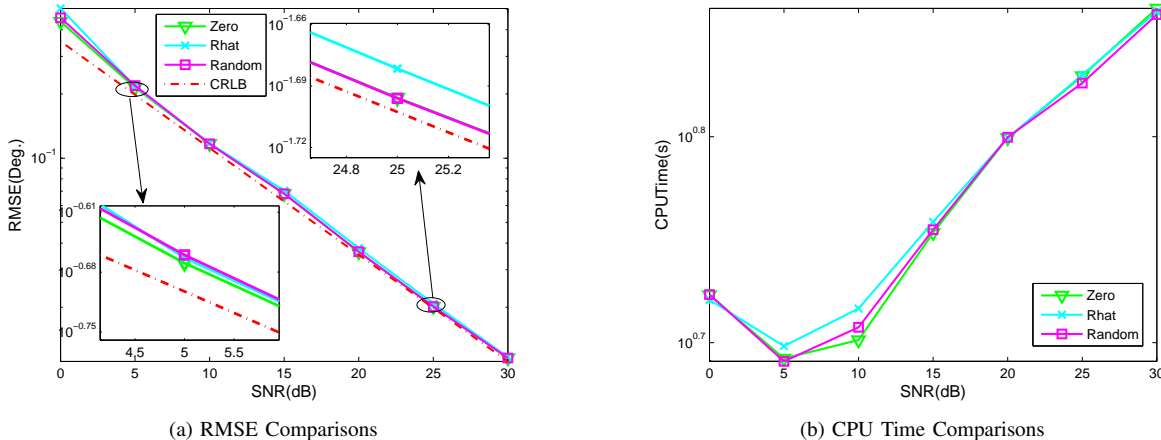


Fig. 10: Performance comparison of ICMRA_{\log} with respect to different initializations for two uncorrelated sources impinging from $[-5^\circ, 5^\circ]$ with the SNR varying from 0dB to 30dB, $L = 200$.

results reveal that this initialization is able to give a satisfactory performance. In this section, we aim to show the superiority of our initialization by empirically exploring the performance of our method with respect to different initializations.

The experiment is carried out on a 7-element ULA, and the parameter setting of this experiment is similar to that of Fig. 6 but with the following different initializations of \mathbf{u}_0 : 1) zero vector, as we have recommended above, 2) random vector with Gaussian distribution, 3) the first column of $\hat{\mathbf{R}}^{\text{full}}$, which can be calculated according to Remark 1. We choose the ICMRA_{\log} for simulation and show the results in Fig. 10 with the SNR varying from 0dB to 30dB. It can be observed that the performance of ICMRA_{\log} with respect to different initializations show similar performance in terms of both RMSE and CPU time. In particular, Fig. 10(b) and the subfigures in Fig. 10(a) indicate that the zero vector initialization that we employed is slightly better than the other two initializations, especially in the middle SNR range. Finally, it can be concluded that our method ICMRA_{\log} using the iterative procedure is insensitive to the initialization. The simulation results with respect to other penalties and FICMRAs reveal the same conclusion and are omitted.

VII. CONCLUSIONS

In this paper, we have proposed a reweighted method named ICMRA by applying a family of nonconvex penalties on the singular values of the covariance matrix as the sparsity metrics. We have also given the convergence analysis of the proposed method as well as two fast implementation algorithms. We have shown that ICMRA can be considered as a sparsity-based method with infinite number of sampling grids. The proposed ICMRA can enhance sparsity and resolution compared to CMRA, as verified through simulations. In our future studies, we will extend the proposed method into the case of generalized arrays. We will be specifically interested in the case where the sensors of an array can be arbitrarily located without being restricted to the half-wavelength sensor spacing,

which is the limitation of the subspace-based methods and the SCMR methods.

APPENDIX A PROOF OF THEOREM 1

To prove Theorem 1, we introduce the following lemma.

Lemma 1 ([36]): Assume $\mathcal{G}^\epsilon[T(\mathbf{u})] = \sum_i g^\epsilon[\sigma_i[T(\mathbf{u})]]$. If g^ϵ is twice differentiable, strictly concave, and $g^{\epsilon\prime\prime}(x) \leq -m_u < 0$ for any bounded u and $0 \leq x \leq u$, then $\mathcal{G}^\epsilon[T(\mathbf{u})]$ is strictly concave, and for any bounded $\mathbf{u}, \mathbf{v} \in \mathbb{R}^N$, $\mathbf{u} \neq \mathbf{v}$, there is some $m > 0$ such that

$$\mathcal{G}^\epsilon[T(\mathbf{u})] - \mathcal{G}^\epsilon[T(\mathbf{v})] \leq \langle T(\mathbf{u} - \mathbf{v}), \nabla \mathcal{G}^\epsilon[T(\mathbf{v})] \rangle - \frac{m}{2} \|T(\mathbf{u} - \mathbf{v})\|_F^2. \quad (41)$$

We first show that $\mathcal{G}^\epsilon[T(\mathbf{u}_j)]$ is convergent. According to Lemma 1 and the concavity of $\mathcal{G}^\epsilon[T(\mathbf{u})]$, we have

$$\mathcal{G}^\epsilon[T(\mathbf{u}_{j+1})] - \mathcal{G}^\epsilon[T(\mathbf{u}_j)] \leq \text{tr}[\nabla \mathcal{G}^\epsilon[T(\mathbf{u}_j)](T(\mathbf{u}_{j+1} - \mathbf{u}_j))] - \frac{m}{2} \|T(\mathbf{u}_{j+1} - \mathbf{u}_j)\|_F^2, \quad (42)$$

which directly results in,

$$\mathcal{G}^\epsilon[T(\mathbf{u}_j)] - \mathcal{G}^\epsilon[T(\mathbf{u}_{j+1})] \geq \text{tr}[\nabla \mathcal{G}^\epsilon[T(\mathbf{u}_j)](T(\mathbf{u}_j - \mathbf{u}_{j+1}))]. \quad (43)$$

Then, since \mathbf{u}_{j+1} is updated according to model (17), we can conclude that,

$$\text{tr}[\nabla \mathcal{G}^\epsilon[T(\mathbf{u}_j)]T(\mathbf{u}_{j+1})] \leq \text{tr}[\nabla \mathcal{G}^\epsilon[T(\mathbf{u}_j)]T(\mathbf{u}_j)], \quad (44)$$

which together with (43) confirms that

$$\mathcal{G}^\epsilon[T(\mathbf{u}_j)] - \mathcal{G}^\epsilon[T(\mathbf{u}_{j+1})] \geq 0. \quad (45)$$

Further, because $\mathcal{G}^\epsilon[T(\mathbf{u})] = \sum_i g^\epsilon[\sigma_i[T(\mathbf{u})]] \geq 0$, the first property can be drawn.

To prove the second property, we first show that the sequence $\{\mathbf{u}_j\}$ is convergent. We start by applying Lemma 1 on $\mathcal{G}^\epsilon[T(\mathbf{u})]$ to get,

$$\begin{aligned} & \mathcal{G}^\epsilon[T(\mathbf{u}_j)] - \mathcal{G}^\epsilon[T(\mathbf{u}_{j+1})] \\ & \geq \text{tr}[\nabla \mathcal{G}^\epsilon[T(\mathbf{u}_j)](T(\mathbf{u}_j - \mathbf{u}_{j+1}))] + \frac{m}{2} \|T(\mathbf{u}_{j+1} - \mathbf{u}_j)\|_F^2 \\ & \geq \frac{m}{2} \|T(\mathbf{u}_{j+1} - \mathbf{u}_j)\|_F^2. \end{aligned} \quad (46)$$

Summing the inequality above for all $j \geq 0$ gives

$$\frac{m}{2} \sum_{j=0}^{+\infty} \|T(\mathbf{u}_{j+1} - \mathbf{u}_j)\|_F^2 \leq \mathcal{G}^\epsilon[T(\mathbf{u}_0)], \quad (47)$$

which implies that $\lim_{j \rightarrow +\infty} T(\mathbf{u}_{j+1} - \mathbf{u}_j) = \mathbf{0}$. Hence the sequence $\{\mathbf{u}_j\}$ is convergent.

To prove that $\{\mathbf{u}_j\}$ converges to a local minimum, we first note that when it converges, i.e., $\mathbf{u}_j \rightarrow \mathbf{u}^*$ as $j \rightarrow \infty$, the models (15) and (17) have the same KKT conditions. This is because the constraints and the derivatives of the objective functions in the two models are the same when the MM method converges. Further, since the objective function in (15) monotonically decreases [36], we can confirm that \mathbf{u}^* is a local minimum of (15). This completes the proof.

REFERENCES

- [1] J. Benesty, J. Chen, and Y. Huang, *Microphone array signal processing*. Springer, 2008, vol. 1.
- [2] J. Picheral and U. Spagnolini, "Angle and delay estimation of space-time channels for TD-CDMA systems," *IEEE Transactions on Wireless Communications*, vol. 3, no. 3, pp. 758–769, May 2004.
- [3] Y. Gu and A. Leshem, "Robust adaptive beamforming based on interference covariance matrix reconstruction and steering vector estimation," *IEEE Transactions on Signal Processing*, vol. 60, no. 7, pp. 3881–3885, July 2012.
- [4] H. Krim and M. Viberg, "Two decades of array signal processing research: the parametric approach," *IEEE Signal Processing Magazine*, vol. 13, no. 4, pp. 67–94, 1996.
- [5] D. H. Johnson and D. E. Dudgeon, *Array signal processing: concepts and techniques*. Simon & Schuster, 1992.
- [6] D. Donoho, "Compressed sensing," *IEEE Transactions on Information Theory*, vol. 52, no. 4, pp. 1289–1306, April 2006.
- [7] D. Malioutov, M. Çetin, and A. S. Willsky, "A sparse signal reconstruction perspective for source localization with sensor arrays," *IEEE Transactions on Signal Processing*, vol. 53, no. 8, pp. 3010–3022, 2005.
- [8] M. M. Hyder and K. Mahata, "Direction-of-arrival estimation using a mixed $l_{2,0}$ norm approximation," *IEEE Transactions on Signal Processing*, vol. 58, no. 9, pp. 4646–4655, 2010.
- [9] Z.-M. Liu, Z.-T. Huang, and Y.-Y. Zhou, "An efficient maximum likelihood method for direction-of-arrival estimation via sparse bayesian learning," *IEEE Transactions on Wireless Communications*, vol. 11, no. 10, pp. 1–11, October 2012.
- [10] —, "Array signal processing via sparsity-inducing representation of the array covariance matrix," *IEEE Transactions on Aerospace and Electronic Systems*, vol. 49, no. 3, pp. 1710–1724, July 2013.
- [11] J. Yin and T. Chen, "Direction-of-arrival estimation using a sparse representation of array covariance vectors," *IEEE Transactions on Signal Processing*, vol. 59, no. 9, pp. 4489–4493, Sept 2011.
- [12] X. Wu, W.-P. Zhu, and J. Yan, "Direction of arrival estimation for off-grid signals based on sparse bayesian learning," *IEEE Sensors Journal*, vol. 16, no. 7, pp. 2004–2016, April 2016.
- [13] Z. Yang, L. Xie, and C. Zhang, "Off-grid direction of arrival estimation using sparse bayesian inference," *IEEE Transactions on Signal Processing*, vol. 61, no. 1, pp. 38–43, Jan 2013.
- [14] H. Zhu, G. Leus, and G. Giannakis, "Sparsity-cognizant total least-squares for perturbed compressive sampling," *IEEE Transactions on Signal Processing*, vol. 59, no. 5, pp. 2002–2016, May 2011.
- [15] Z. Tan, P. Yang, and A. Nehorai, "Joint sparse recovery method for compressed sensing with structured dictionary mismatches," *IEEE Transactions on Signal Processing*, vol. 62, no. 19, pp. 4997–5008, Oct 2014.
- [16] V. Chandrasekaran, B. Recht, P. A. Parrilo, and A. S. Willsky, "The convex geometry of linear inverse problems," *Foundations of Computational Mathematics*, vol. 12, no. 6, pp. 805–849, 2012.
- [17] G. Tang, B. Bhaskar, P. Shah, and B. Recht, "Compressed sensing off the grid," *IEEE Transactions on Information Theory*, vol. 59, no. 11, pp. 7465–7490, Nov 2013.
- [18] Z. Yang and L. Xie, "On gridless sparse methods for line spectral estimation from complete and incomplete data," *IEEE Transactions on Signal Processing*, vol. 63, no. 12, pp. 3139–3153, June 2015.
- [19] D. M. Wikes and M. H. Hayes, "Iterated Toeplitz approximation of covariance matrices," in *International Conference on Acoustics, Speech, and Signal Processing, 1988. ICASSP-88., 1988*, Apr 1988, pp. 1663–1666 vol.3.
- [20] B. Ottersten, P. Stoica, and R. Roy, "Covariance matching estimation techniques for array signal processing applications," *Digital Signal Processing*, vol. 8, no. 3, pp. 185–210, 1998.
- [21] H. Li, P. Stoica, and J. Li, "Computationally efficient maximum likelihood estimation of structured covariance matrices," *IEEE Transactions on Signal Processing*, vol. 47, no. 5, pp. 1314–1323, May 1999.
- [22] P. Stoica, P. Babu, and J. Li, "New method of sparse parameter estimation in separable models and its use for spectral analysis of irregularly sampled data," *IEEE Transactions on Signal Processing*, vol. 59, no. 1, pp. 35–47, Jan 2011.
- [23] Z. Yang, L. Xie, and C. Zhang, "A discretization-free sparse and parametric approach for linear array signal processing," *IEEE Transactions on Signal Processing*, vol. 62, no. 19, pp. 4959–4973, Oct 2014.
- [24] Y. Li and Y. Chi, "Off-the-grid line spectrum denoising and estimation with multiple measurement vectors," *IEEE Transactions on Signal Processing*, vol. 64, no. 5, pp. 1257–1269, March 2016.
- [25] X. Wu, W. P. Zhu, and J. Yan, "Direction-of-arrival estimation based on Toeplitz covariance matrix reconstruction," in *2016 IEEE International Conference on Acoustics, Speech and Signal Processing (ICASSP)*, March 2016, pp. 3071–3075.
- [26] —, "A Toeplitz covariance matrix reconstruction approach for direction-of-arrival estimation," *IEEE Transactions on Vehicular Technology*, vol. 66, no. 9, pp. 8223–8237, Sept 2017.
- [27] S. Oymak, K. Mohan, M. Fazel, and B. Hassibi, "A simplified approach to recovery conditions for low rank matrices," in *IEEE International Symposium on Information Theory Proceedings (ISIT), 2011*, July 2011, pp. 2318–2322.
- [28] M. Malek-Mohammadi, M. Babaie-Zadeh, and M. Skoglund, "Performance guarantees for Schatten- p quasi-norm minimization in recovery of low-rank matrices," *Signal Processing*, vol. 114, no. C, pp. 225–230, 2014.
- [29] M. Fazel, H. Hindi, and S. P. Boyd, "Log-det heuristic for matrix rank minimization with applications to hankel and euclidean distance matrices," in *American Control Conference, 2003. Proceedings of the 2003*, vol. 3, June 2003, pp. 2156–2162 vol.3.
- [30] K. Mohan and M. Fazel, "Iterative reweighted algorithms for matrix rank minimization," *Journal of Machine Learning Research*, vol. 13, no. 13, pp. 3441–3473, 2012.
- [31] J. Trzasko and A. Manduca, "Highly undersampled magnetic resonance image reconstruction via homotopic ℓ_0 -minimization," *IEEE Transactions on Medical Imaging*, vol. 28, no. 1, pp. 106–121, Jan 2009.
- [32] Z.-M. Liu, Z.-T. Huang, and Y.-Y. Zhou, "Sparsity-inducing direction finding for narrowband and wideband signals based on array covariance vectors," *IEEE Transactions on Wireless Communications*, vol. 12, no. 8, pp. 1–12, August 2013.
- [33] J. Fan and R. Li, "Variable selection via nonconcave penalized likelihood and its oracle properties," *Journal of the American Statistical Association*, vol. 96, no. December, pp. 1348–1360, 2001.
- [34] C. H. Zhang, "Nearly unbiased variable selection under minimax concave penalty," *Annals of Statistics*, vol. 38, no. 2, pp. 894–942, 2010.
- [35] C. Lu, J. Tang, S. Yan, and Z. Lin, "Nonconvex nonsmooth low rank minimization via iteratively reweighted nuclear norm," *IEEE Transactions on Image Processing*, vol. 25, no. 2, pp. 829–839, Feb 2016.
- [36] M. Malek-Mohammadi, M. Babaie-Zadeh, and M. Skoglund, "Iterative concave rank approximation for recovering low-rank matrices," *IEEE Transactions on Signal Processing*, vol. 62, no. 20, pp. 5213–5226, Oct 2014.
- [37] Z. Yang and L. Xie, "Enhancing sparsity and resolution via reweighted atomic norm minimization," *IEEE Transactions on Signal Processing*, vol. 64, no. 4, pp. 995–1006, Feb 2016.

- [38] M. S. Asif and J. Romberg, "Sparse recovery of streaming signals using ℓ_1 -homotopy," *IEEE Transactions on Signal Processing*, vol. 62, no. 16, pp. 4209–4223, Aug 2014.
- [39] S. Boyd and L. Vandenberghe, *Convex optimization*. Cambridge university press, 2004.
- [40] R. Schmidt, "Multiple emitter location and signal parameter estimation," *IEEE Transactions on Antennas and Propagation*, vol. 34, no. 3, pp. 276–280, 1986.